An Analysis of Polygenes Affecting Wing Shape on Chromosome 2 in *Drosophila melanogaster*

Kenneth Weber,* Robert Eisman,* Shawn Higgins,* Lisa Morey,* April Patty,* Michele Tausek* and Zhao-Bang Zeng†

**Department of Biological Sciences, University of Southern Maine, Portland, Maine 04104-9300 and †Department of Statistics, North Carolina State University, Raleigh, North Carolina 27695-8203*

Manuscript received February 22, 2001
Accepted for publication August 3, 2001

ABSTRACT

Genetic effects on an index of wing shape on chromosome 2 of *Drosophila melanogaster* were mapped using isogenic recombinants with transposable element markers. At least 10 genes with small additive effects are dispersed evenly along the chromosome. Many interactions exist, with only small net effects in homozygous recombinants and little effect on phenotypic variance. Heterozygous chromosome segments show almost no dominance. Pleiotropic effects on leg shape are only minor. At first view, wing shape genes form a rather homogeneous class, but certain complexities remain unresolved.

THE genetic control of organ shapes in development can be analyzed using metrics that eliminate the allometric effect of size. For example, wing shape in *Drosophila melanogaster* can be quantified by the angular deviations of individual wings from baselines that represent the average shape in a base population. Each baseline approximates the centerline of a scatterplot of two dimensions in wild-type flies over a nearly twofold range of body size caused by temperatures from 18° to 30° and by starvation (Weber 1990). Angular offsets from these baselines are independent of most environmental body size effects. Analyses using this method have demonstrated many intriguing features of wing shape genes.

Wing shape is highly selectable. Lines selected divergently for various wing angular offsets showed a mean realized heritability of ~0.35 and a final mean divergence of ~15 phenotypic standard deviations (Weber 1990). Wing shape is controlled by numerous genes, as shown by statistical analysis of selection lines (Weber 1990) and by mapping of quantitative trait loci (QTL; Weber *et al.* 1999). Some of these genes act within separate localized regions of the wing. When any two dimensions were selected antagonistically to each other, it was possible to change them both oppositely at the same time, in either direction, thus allowing rather plastic deformation of the wing (Weber 1990). Moreover, some genes can affect the shapes of surprisingly small, localized regions of the wing without having proportional effects outside those regions (Weber 1992). Selected lines show changes both in the sizes of intervein areas and in the locations of vein intersections (Weber 1990, 1992). The effects of wing shape genes are strikingly independent of wing size in that flies of a defined genetic line retain the same approximate mean trait value over at least a 20% range in wing dimensions. Even lines with highly selected wing shapes that are many standard deviations outside the range of wild type show this constancy of shape regardless of size (Weber 1990; Weber *et al.* 1999). Wing shape genes also act largely independently of sex; that is, when shape is measured relative to baselines derived separately for each sex, the offsets of selected males and females from their respective baselines remain almost identical in every selected shape trait (Weber 1990). Wing shape is strongly resistant to environmental influences that cause intergenerational variation, and this resistance is also preserved in extreme selected genotypes (Weber 1990). Probably only Castle's results on rat fur color (Castle and Phillips 1914; Castle 1951) show selected changes freer of intergenerational environmental influences. Wing shape genes show little dominance in that hybrids between different genotypes have nearly intermediate phenotypes (Weber *et al.* 1999). They are also highly additive in that the phenotypic variance is nearly equal to the sum of the additive genetic variance, as measured in selection experiments, and of the environmental variance, as measured in long-inbred lines (Weber 1990). Wing shape genes have only minor interactions with fitness: Highly selected lines can be made isogenic with no loss of the phenotype and little loss of viability (K. Weber, unpublished data), and highly inbred lines show high between-line variance in wing shape (Weber 1990). Wing shape genes also have little correlated effect on the shapes of other appendages (Weber *et al.* 1999).

These general observations have exceptions and should be qualified. For example, in one selection line a major shape gene with a large correlated effect on

Corresponding author: K. Weber, Department of Biological Sciences, University of Southern Maine, Box 9300, Portland, ME 04104-9300. E-mail: keweber@usm.maine.edu

body size appeared (Weber 1990), and small correlated effects on size appeared in several other lines. In another line, a major shape gene appeared that also caused female sterility (Weber 1990). There are significant sources of environmental variance in nature in that phenotypic variances in wing shape are on average 47% higher in wild-caught flies than in their lab-reared offspring (Weber 1990). Multiple interval mapping (MIM) analysis of chromosome 3 provides evidence of possibly strong pairwise QTL interactions (Weber *et al.* 1999). Finally, wing shape does not respond to selection with perfect plasticity but shows some correlations among dimensions (Weber 1990; see also Guerra *et al.* 1997).

Several of these observations have since been confirmed by others using different approaches. Birdsall *et al.* (2000) performed shape analyses of three intervein regions in *D. melanogaster* using the morphometric method of relative warps (Bookstein 1991), comparing inbred lines at 18° and 25°. Each wing region varied independently of the others in a genotype-specific way, confirming the existence of shape control by locally acting genes. The two temperatures caused differences in wing area of up to 20%, but the shape parameters of each wing region tended to remain constant within each inbred line at both wing sizes, confirming the wing-size independence of shape genes. The effects of sex also tended to be constant across genotypes. Some shape parameters in some wing regions showed departures from perfect size and sex independence. Zimmerman *et al.* (2000) followed Birdsall *et al.* (2000) with QTL analyses of wing shape, using the same intervein regions, shape parameters, and temperatures. This confirmed again the presence of locally acting genes and the relative independence of wing shape gene effects from sex and size. Dominance among QTL was assessed for one intervein region and found to be mostly negligible. These studies indicate that the analysis of shape genes will result in similar conclusions when any size-independent shape metric is used.

Wing shape is an ideal trait for quantitative genetic analysis, and angular offsets are convenient for their simplicity. Angular offsets of wing shape have normal distributions and nearly constant variances, even when selection greatly changes the mean (Weber 1990). Selected phenotypes remain stable for many years. The most convenient feature is the remarkable resistance to environmental fluctuations, seen in the smooth graphs of selection response (Weber 1990). It is also convenient that both sexes always have nearly identical angular offsets (from slightly different baselines) so that comparisons can be made using a single sex.

With the publication of a QTL analysis of the third chromosome (Weber *et al.* 1999), wing shape became the third morphological trait in *D. melanogaster*, after bristle number (Long *et al.* 1995) and features of the male genital arch (Liu *et al.* 1996), to be analyzed by current methods of QTL mapping. Here we extend our investigation to chromosome 2. With these two studies, we have now covered ~80% of the genome and 90% of the total phenotypic difference between the "high" and "low" lines produced by 20 generations of divergent selection on this representative wing shape trait, arbitrarily designated "index F" (Weber 1990). The remaining 10% of the phenotypic difference arises from chromosome 1 (the X chromosome), which is still being analyzed.

This study attains a higher resolution of small genetic effects than was possible for chromosome 3. The data set of 35,050 measured wings from 701 recombinant isogenic lines is 35% larger than the data set for chromosome 3 (Weber *et al.* 1999). Moreover, the variance among line means with the same marker genotype is ~40% lower for chromosome 2 than it was for chromosome 3, probably due to improved consistency among measurement technicians. The increases in accuracy and number of measurements and the high density of markers (110 cM/47 markers) permit a resolution of effects that is powerful for this type of study. The outlines of the system of polygenic shape control are revealed. Nevertheless, we find that because of the high density of genetic effects, even higher resolution would be required to quantify the numbers and effects with acceptable confidence.

MATERIALS AND METHODS

This study used the same experimental methods as the previous study of chromosome 3 (Weber *et al.* 1999). Second chromosomes were derived from lines previously selected for high or low values of an index of wing shape. A line that was isogenic for the high (H) second chromosome and for the low (L) first and third chromosomes (L-H-L) was crossed to another line that was isogenic low in all three chromosomes (L-L-L). Random recombinants between the high and low second chromosomes were then extracted and made homozygous again in the same background of isogenic low first and third chromosomes by using a third stock with isogenic low first and third chromosomes and a balancer second chromosome (L-B-L). The balancer chromosome was *SM5* (Lindsley and Zimm 1992) with *Curly*^{0}/*Sternopleural*.

The high and low second chromosomes could be differentiated by the line-specific insertion sites of the transposable element *roo*, identified by *in situ* labeling of salivary gland chromosome squashes. Three additional marker sites in one region were gained by using the transposable element *jockey*. The sites of second-chromosome insertion markers are listed in Table 1.

One left or right wing at random was measured from each of 50 males per line. Only males were measured because male and female offsets (from different baselines) are nearly identical and respond equally to selection (Weber 1990). Wing measurements were made on whole flies by projecting wings onto a digitizer pad with a microprojector (Weber 1988; Weber *et al.* 1999).

The phenotypic scale: As in previous studies, wing (and leg) shapes were quantified using indexes based on two dimensions, D_1 and D_2. In the wing shape index used here (designated index F), D_1 is the width across the middle of the wing and D_2 is the width across the base, using vein intersections as

TABLE 1

Marker sites on chromosome 2

Band	Chromosome	cM	Band	Chromosome	cM	Band	Chromosome	cM
22A2	H	2.2	37B8	L	53.7	47B4	L	60.3
22B2	H	2.4	37D1	H	53.9	47D1	L	60.9
23B1	H	6.6	38D1	H	54.6	48D1	H	62.5
23C3	L	7.5	38E1	H	54.7	49E4	H	66.7
24C1	H	10.3	39E1	H	54.9	50D1	H	70.8
24D4	H	11.2	41D1	H	55.5	*51D6*	H	73.5
24E5	L	12.0	42B1	L	55.6	*52A1*	L	74.6
25A1	L	13.0	42B2	H	55.7	*55C4*	H	83.8
25A3	H	13.5	42C1	L	55.8	56B7	H	87.5
27B1	H	19.8	42C3	L	55.9	56F3	H	90.0
29F1	H	30.4	43A1	L	56.4	57E6	H	98.1
32C1	L	42.9	43B3	L	56.5	58D1	L	99.2
33A1	H	44.3	44F1	H	58.3	59A1	L	101.7
34A5	H	46.2	46C1	L	59.7	59B8	L	102.3
34B2	H	46.5	46C6	H	59.8	60F1	L	108.1
35B6	L	50.4	46F1	H	60.0			

Band positions of 44 nonidentical *roo* insertion sites, plus 3 *jockey* insertion sites (in italics) appearing on either the high or the low chromosome 2 (genetic map positions in centimorgans).

landmarks (See Weber 1990, Figure 1). To derive a shape index, two dimensions from each individual are first transformed into polar coordinates [$\theta = \arctan(D_2/D_1)$ and $r = (D_1^2 + D_2^2)^{1/2}$; thus, $D_1 = r\cos\theta$ and $D_2 = r\sin\theta$]. The value of the shape index is then the *angular offset* expressed in radians of the point (D_1, D_2) from a reference baseline. The reference baseline represents the mean allometric relation between the dimensions D_1 and D_2 in the base population. The baseline has the formula $\theta = \beta r^{\alpha}$ and is derived from wild-type flies by the regression of $\log(\theta)$ on $\log(r)$, after conversion of each point (D_1, D_2) to polar coordinates. For index *F*, $\beta = 0.4048$ and $\alpha = -0.043$ (Weber 1990). Individuals that deviate from the base population allometry have either positive (clockwise) or negative (counterclockwise) offsets from the baseline. Individuals falling exactly on the baseline have angular offsets of zero. Variations in body proportions change the angular offset only if they cause deviations from the baseline curve. This cancels the confounding effect of variations in body size.

Measurement of legs: Legs of lines L-H-L and L-L-L were mounted on slides in glycerol under coverslips and sealed with fingernail polish. Left legs were mounted with anterior side upward and flexed femorotibial joint. On legs thus mounted, D_1 is the width of each segment at its widest point, and D_2 is the width of the same segment at its narrowest point, which is more proximal. These were essentially the same dimensions used previously (Weber *et al.* 1999) but were very slightly redefined for this study. Therefore, the measurements of L-L-L leg segments were repeated from a new sample for this comparison of L-H-L to L-L-L. Mounted legs were projected and digitized in the same way as wings.

Multiple interval mapping analysis: The method of MIM analysis follows Kao *et al.* (1999), Zeng *et al.* (1999), and Weber *et al.* (1999) with some modifications. Briefly, a multiple QTL model is used to search for the number, positions, and epistatic terms of QTL in a stepwise fashion. In each step, the analysis first searches for the position of a new putative QTL and tests it for significance using the residual permutation test (Zeng *et al.* 1999); it then updates the estimate of position for each selected QTL conditional on other QTL in a sequential way. This process is repeated until no new QTL is detected on the basis of the residual permutation test. The initial model for the MIM analysis is provided by a backward stepwise regression on markers with $\alpha = 0.01$ as the critical level for the test of partial regression coefficients.

The residual permutation test compares a model with k QTL, regarded as the null hypothesis, and a model with $k + 1$ QTL that contains the k QTL model, regarded as the alternative hypothesis. We first obtained the estimated genotypic value for each individual under the null hypothesis (the k QTL model). We then randomly shuffled the residuals (the difference between the observed phenotypic value and the estimated genotypic value under the null hypothesis) among individuals to obtain a residual permutation sample. Next we searched for a putative QTL conditional on the k QTL in the residual permuted sample and recorded the maximum test statistic. This resampling and search was performed a number of times (500) to obtain an empirical 95% significance threshold. To decide whether to accept the new QTL, we compared this threshold to the test statistic for the $(k + 1)$th QTL in the original sample.

After selecting the QTL number and positions, a backward stepwise-selection procedure was used to select a subset of significant QTL additive-by-additive interaction effects. In each step, an epistatic effect that is the least significant by a likelihood-ratio test is dropped from the model. The process is repeated until each remaining epistatic effect is significant by the likelihood-ratio test conditional on other QTL effects.

RESULTS

The data set comprises the phenotypic means and recombination breakpoints of 701 isogenic recombinant second-chromosome lines with the same background of isogenic low first and third chromosomes. The measured lines are distributed among single recombinants (217 HL and 256 LH), double recombinants (79 HLH and 99 LHL), triple recombinants (4 HLHL and 6 LHLH), and nonrecombinants (20 H and 20 L).

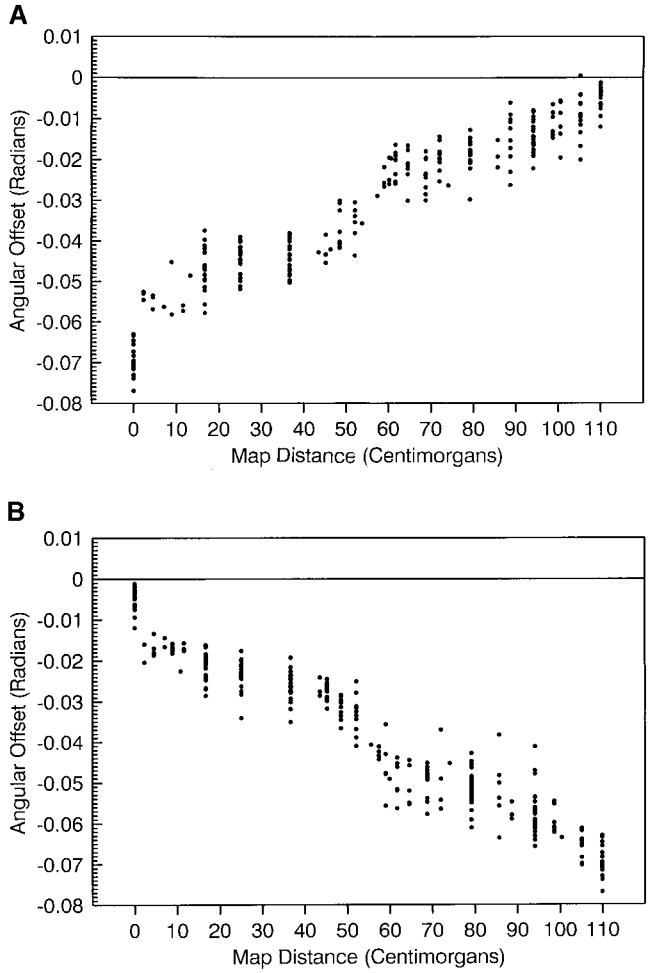

FIGURE 1.—Phenotypes of single recombinant and nonrecombinant lines as a function of breakpoint in centimorgans. Breakpoints are estimated as the midpoints between markers showing recombination. (A) Phenotypes of 217 high-low single recombinants, 20 low nonrecombinants, and 20 high nonrecombinants. (B) Phenotypes of 256 low-high single recombinants, the same 20 low nonrecombinants, and the same 20 high nonrecombinants.

(Many more nonrecombinants were recovered but not measured.)

Reduction in variance between lines: Variances between line means with the same marker genotype were higher for the third chromosome (WEBER *et al.* 1999) than for the second chromosome (this study). For the third chromosome, the mean of the variance between nonrecombinant high lines and the variance between nonrecombinant low lines was 1.6×10^{-5}, and the weighted mean variance between single recombinant lines of the same marker genotype, among all genotypes with more than two lines, was 2.9×10^{-5}. For the second chromosome, the mean variance between nonrecombinant lines was 1.0×10^{-5}, and the weighted mean variance between single recombinant lines of the same marker genotype, among all genotypes with more than two lines, was 1.8×10^{-5}. Thus, in this study, same-genotype variances declined by 37.5% among nonrecombinants and by 37.9% among single recombinants. This would not be expected because the mean map distance between markers for chromosome 2 is actually a little larger (2.3 cM/marker) than it was for chromosome 3 (1.8 cM/marker). The greater consistency of same-genotype measurements for chromosome 2 probably resulted from our intensive efforts to eliminate small differences among operators in the exact digitizing of landmarks.

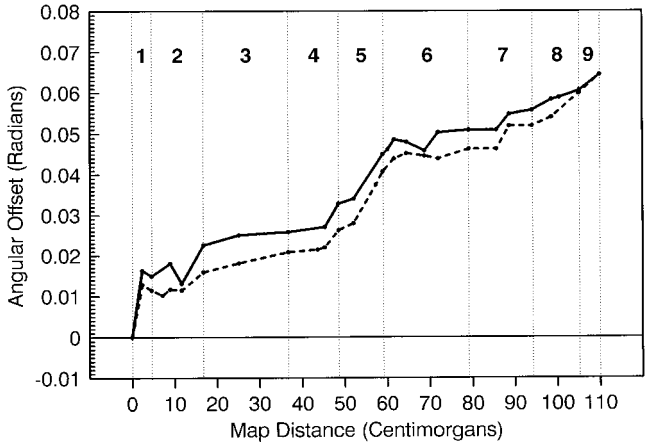

FIGURE 2.—Graphic analysis of single recombinant lines. Mean phenotypic effects of high-low (solid line) and low-high (dashed line) single recombinants from Figure 1 are shown. Both curves show the absolute cumulative effect of genes along the chromosome as a positive deviation from the left end, so that the descending low-high profile of Figure 1 is inverted to parallel the rising high-low profile. Serial *t*-tests of single recombinant means (Table 2) divide the chromosome into nine segments with differentiable genetic effects (vertical lines).

Single recombinants: Figure 1 shows the phenotypes of all single recombinant and nonrecombinant lines as a function of recombination breakpoint. Both graphs show the incremental accumulation of genetic effects along the chromosome. The two profiles of cumulative effect can be directly compared by using the mean absolute value of their increasing deviation from the left-end phenotypic mean (Figure 2), *i.e.*, as values of HL-L and H-LH. Changes in slope differentiate regions with larger or smaller effect. Because the two profiles in Figure 2 follow nearly the same pattern, it is apparent that switching a segment between H and L usually has about the same effect, whether the segment is flanked by H on the left and L on the right (HXL) or the reverse (LXH). In other words, these genes appear to act largely independently of each other.

A series of *t*-tests on the set of all single recombinants and nonrecombinants separates the chromosome into nine segments with significant effects (Figure 2 and Table 2). This is a minimum estimate of the number of genes. The segments are somewhat alike in size but smaller at the ends of the chromosome. They do not correspond to distinct steps in the profiles of cumulative effect.

TABLE 2

Nine chromosome segments with separable genetic effects

	LH			HL				
cM	*n*	Mean	SD	*n*	Mean	SD	Segment	Effect
0.0	20	−0.0053	±0.00266	20	−0.0697	±0.00354		
							1	0.0132
4.5	4	−0.0168	±0.00233	3	−0.0548	±0.00186		
							2	0.0060
16.7	28	−0.0212	±0.00345	23	−0.0472	±0.00488		
							3	0.0041
36.7	27	−0.0261	±0.00383	26	−0.0439	±0.00376		
							4	0.0062
48.5	10	−0.0315	±0.00271	8	−0.0369	±0.00499		
							5	0.0134
59.0	5	−0.0460	±0.00735	3	−0.0247	±0.00255		
							6	0.0058
79.2	37	−0.0516	±0.00358	12	−0.0188	±0.00433		
							7	0.0052
94.1	24	−0.0572	±0.00561	23	−0.0140	±0.00386		
							8	0.0064
105.2	12	−0.0652	±0.00304	12	−0.0092	±0.00572		
							9	0.0042
110.0	20	−0.0697	±0.00354	20	−0.0053	±0.00266		

Separation of chromosome 2 into nine segments by breakpoints with significantly different phenotypic means. At each interval, $P < 0.001$ by combined *t*-tests. For each breakpoint the table shows map locations in centimorgans, numbers (n) of single recombinant lines (LH or HL), and mean ±SD of each set of n line means. Samples at 0.0 and 110.0 cM are the same but in reversed positions. Effect is the mean effect of each segment.

The net effect of interactions across any point of the chromosome can be quantified by subtracting the HL profile from the LH profile in Figure 2. This net effect is always negative, with a roughly constant value and a mean of −0.0042. Considering the nearly parallel profiles along most of the chromosome, the simplest model would be a single pairwise interaction between loci near 2 and 105 cM, with an effect of −0.0042. However, examination of the double recombinants shows that the situation is more complicated.

Double recombinants: The double recombinants are numerous enough to merit a separate graphic analysis. Double recombinants can be graphed as a surface, where x is the first breakpoint, y is the second breakpoint, and z is the mean phenotype of double recombinant lines with breakpoints x and y (Figure 3). All possible double recombinants fall on the surface above the triangle ($0 \le x \le 110$, $0 \le y \le 110$, $x \le y$). There is one surface for HLH double recombinants and another for LHL. The two surfaces can be compared best when represented as positive deviations from opposite ends of the phenotypic range: HLHs as H-HLH, and LHLs as LHL-L. This inverts the HLH surface so that both surfaces have the same basic shape.

This convention represents not only double recombinants but also single recombinants and nonrecombinants, on a surface of absolute effect. Single recombinants appear in Figure 3 in the two vertical planes along the sides. For example, an LH single recombinant can be regarded either as an LHL double recombinant with the second breakpoint at the right end (110 cM) or as an HLH double recombinant with the first breakpoint at the left end (0 cM). Each single recombinant line appears on both these planes. Thus, the plots of single recombinant means shown in Figure 2 are visible again in Figure 3 in the plane $x = 0$ on the left side and in inverted orientation in the plane $x = 110$ on the right side. Nonrecombinants also appear in Figure 3 at the three vertices where the two surfaces converge. For example, H nonrecombinants are equivalent to LHL double recombinants with the first breakpoint at 0 cM and the second breakpoint at 110 cM; and they are also equivalent to HLH double recombinants with both breakpoints at 0 cM or both at 110 cM. The phenotypic surface of z-values descends from a vertex at $x = 0$, $y = 110$ to 0 at all points along the diagonal $x = y$ (where LHL = L and HLH = H). Thus all nonrecombinants and all single recombinants in the data set appear on both the LHL and the HLH surfaces, along with all the double recombinants of either one kind or the other. In fact, the two surfaces in Figure 3 present a natural topography of the whole data set, excluding only the few triple recombinants.

If there were no interactions among loci on the second chromosome, the two surfaces in Figure 3 would be identical. This is the geometrical way of stating that

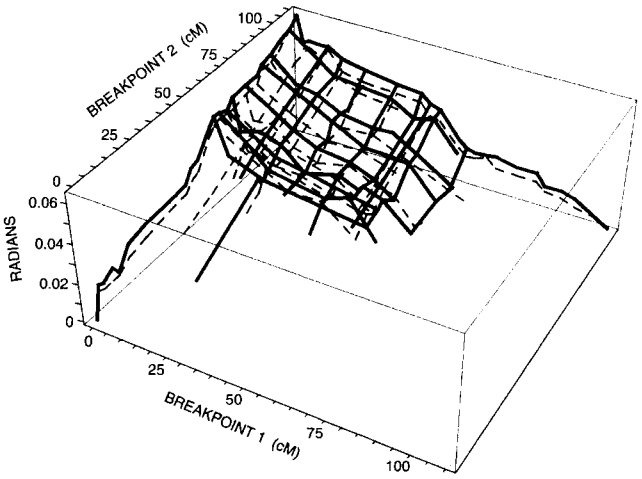

FIGURE 3.—Graphic analysis of the whole data set. The mean phenotypic effects of all double recombinant, single recombinant, and nonrecombinant lines form two surfaces: an LHL surface (solid lines) and an HLH surface (dashed lines). Single recombinants appear in both surfaces along the sides, and nonrecombinants appear at the vertices. The LHL surface is slightly higher than the HLH surface almost everywhere, indicating that the net value of interactions between any segment and its flanking segments is almost always small and negative. The graph represents 165 of the 178 double recombinant lines. Three were excluded because neither breakpoint matched a single recombinant breakpoint; hence, the data points could not be connected to the edge of the graph. One was excluded because it was near the edge and visually ambiguous. Nine were excluded as apparent outliers.

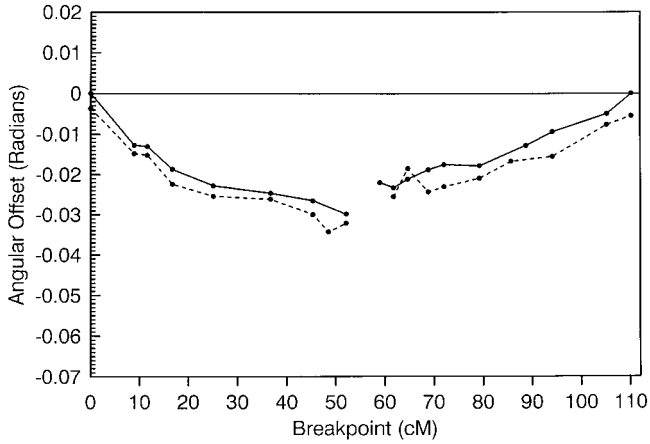

FIGURE 4.—Averages of all parallel vertical cross sections through the surfaces in Figure 3, presented in two perpendicular views to show the average separation between the LHL surface (solid lines) and the HLH surface (dashed lines). Before averaging, the offset values in each slice were first converted to negative offsets from the single recombinant mean on the upper (LHL) surface in the vertical plane of each slice. Thus, zero offset represents the outside of the LHL surface in any slice. Left, mean view of all vertical slices parallel to the *x*-axis, varying breakpoint 1. Right, mean view of all vertical slices parallel to the *y*-axis, varying breakpoint 2.

if the genes in the segment between any two breakpoints have no interactions with genes in either flanking segment, then the quantities H-HLH and LHL-L are equal. That is, if any part of the high chromosome is replaced by low, the absolute change in phenotype is the same as if the same part of the low chromosome were replaced by high, as long as no interacting loci change their linkage phase in the exchange. Thus the vertical separation between the HLH and LHL surfaces (subtracting the latter from the former) at any point (x, y) gives the sign and magnitude of the net of all those interactions where genes located between the breakpoints (x and y) interact with genes located outside the breakpoints.

Most double recombinants have one breakpoint in each chromosome arm; very few have both in the same arm. Therefore, the data in Figure 3 are mainly confined to the square central area of the *xyz* surface where $x <$ 55 cM (the approximate centromere) and $y >$ 55 cM. Figure 3 shows that in this area the surfaces are separated almost everywhere by roughly constant intervals. This is revealed more clearly by Figure 4.

The graphed double recombinants show that a welter of interactions exists, with mostly negative net effects. They also agree with the single recombinants, in that all detectable net effects of interactions in homozygous recombinants are small; *i.e.*, most gene action is independent of the effects of other genes. This is implied by the demonstration that the HLH and LHL surfaces are nearly congruent, as far as the data can show.

Results of multiple interval mapping: Backward stepwise regression selected 11 markers that together explained 93% of the total variance. On the basis of this initial model, the positions of the putative QTL were first scanned and updated sequentially under the hypothesis of 11 QTL. The residual permutation test was then performed for the least-significant QTL. This putative QTL has a LOD score of 1.6 and the 95% residual permutation threshold with a model of the 10 QTL is 3.6 LOD. [This residual permutation threshold is different from and higher than the regular permutation threshold of CHURCHILL and DOERGE (1994), which is 1.7 LOD for the experiment. This is because the residual permutation test is conditional on other QTL and the test statistic in different regions separated by QTL is more or less independent.] This candidate QTL was dropped from the model and the positions of the remaining 10 QTL were optimized again. All these QTL were tested to be significant. A forward search for a new QTL was then attempted, and no significant QTL was found.

Given the 10 QTL and the estimated positions, the search for epistatic terms was performed by a backward stepwise-selection procedure to select a subset of significant QTL additive-by-additive interaction effects. The model started with the 10 additive effects and 45 possible additive-by-additive interaction effects, and the selection proceeded to remove nonsignificant interaction effects one at a time. In most of this search process,

TABLE 3

Estimated QTL positions, LOD scores, additive effects, and additive-by-additive interaction effects

QTL (pair)	Position (cM)	LOD	Effect ($\times 10^2$)	Effect (%)
1	2	102.0	1.35	20.9
2	16	38.2	0.78	12.2
3	37	5.3	0.32	4.9
4	47	14.7	0.54	8.4
5	54	11.5	0.86	13.4
6	58	7.9	0.64	9.9
7	72	11.4	0.35	5.4
8	88	29.2	0.63	9.8
9	98	12.9	0.55	8.5
10	108	7.9	0.37	5.8
(1, 2)		5.7	1.49	
(1, 3)		8.4	−1.10	
(1, 5)		4.6	−0.52	
(1, 9)		3.8	−0.17	
(2, 4)		4.5	1.48	
(2, 5)		3.8	0.27	
(2, 6)		4.5	−0.36	
(2, 8)		2.7	−0.22	
(3, 4)		3.0	−1.08	
(3, 7)		4.7	0.13	
(4, 6)		9.3	0.33	
(8, 9)		3.4	0.73	
(8, 10)		3.1	−0.80	
(9, 10)		3.3	0.89	
Total				99.1

Effects in radians of angular offset. Additive effects are also given as percentages of phenotypic difference between nonrecombinant lines, L-H-L and L-L-L.

not many interaction terms in the models were statistically significant. However, after dropping the 31st least-significant interaction term, all the 14 remaining interaction terms became very significant, conditional on others. The selection process was stopped here, and the final model contains 10 additive effects and 14 additive-by-additive interaction effects. The estimates of positions, additive effects, and additive-by-additive interaction effects of QTL are given in Table 3. The partition of variances and covariances explained by QTL additive effects is given in Table 4, and that explained by QTL epistatic effects is given in Table 5.

Figure 5 gives the likelihood-ratio test statistic profile in LOD score for each QTL conditional on the other QTL effects, including the epistatic effects. This profile shows the strength of statistical evidence for mapping each QTL. It is very difficult to obtain accurate estimates of confidence intervals for QTL positions with multiple QTL (Kao and Zeng 1997). We plot the 1-LOD support interval for each QTL (conditional on the estimates of other QTL), which is the genome region covered by the drop of 1 LOD from the peak in the likelihood profile, to indicate the likely region where the QTL may be located. It is not clear how much confidence the 1-LOD support interval may have in this multidimensional inference.

The estimated additive effects of the 10 QTL are all in one direction, ranging in magnitude from 5 to 21% of the phenotypic difference between the two parental genotypes (Table 3) and summing to 99.1% of the difference. There is good agreement between the observed sum and the expected sum, as the sum of additive effects in the model is assumed to equal the phenotypic difference between the two parental genotypes and is not affected by interactions according to the model.

The additive effects together explain 95.1% of the total phenotypic variance (Table 4), and the epistatic effects together explain only 0.3% of the total variance (Table 5). The covariances between the additive effects and epistatic effects, expected to be zero (Kao *et al.* 1999), are very small (almost zero). The model explains 95.4% of the total variance.

To further support the selection of the model given in Table 3 with the 14 epistatic effects, we show in Table 6 the log likelihoods for a series of models in the backward stepwise elimination process for epistasis. Table 6

TABLE 4

Estimated variances and covariances of QTL additive effects as percentages of total phenotypic variance

QTL	1	2	3	4	5	6	7	8	9	10	Sum
1	16.6	7.0	0.9	0.2	−1.5	−1.1	−0.7	−1.6	−2.2	−1.7	15.6
2	7.0	5.6	1.1	1.1	0.6	0.3	−0.1	−0.6	−1.2	−1.0	12.8
3	0.9	1.1	0.9	1.2	1.4	1.0	0.3	0.1	−0.2	−0.2	6.4
4	0.2	1.1	1.2	2.7	3.5	2.4	0.8	0.6	−0.2	−0.3	11.8
5	−1.5	0.6	1.4	3.5	6.8	4.8	1.6	1.1	−0.2	−0.5	17.4
6	−1.1	0.3	1.0	2.4	4.8	3.7	1.2	0.9	−0.1	−0.3	12.9
7	−0.7	−0.1	0.3	0.8	1.6	1.2	1.1	1.2	0.5	0.2	6.2
8	−1.6	−0.6	0.1	0.6	1.1	0.9	1.2	3.6	2.2	1.2	8.7
9	−2.2	−1.2	−0.2	−0.2	−0.2	−0.1	0.5	2.2	2.8	1.6	3.0
10	−1.7	−1.0	−0.2	−0.3	−0.5	−0.3	0.2	1.2	1.6	1.3	0.3
Total											95.1

TABLE 5

Estimated variances and covariances of QTL additive-by-additive interaction effects in percentages of total phenotypic variance

QTL pair	1, 2	1, 3	1, 5	1, 9	2, 4	2, 5	2, 6	2, 8	3, 4	3, 7	4, 6	8, 9	8, 10	9, 10	Sum
1, 2	2.4	−1.2	−0.4	0.0	−0.9	−0.2	0.2	0.1	0.2	0.0	0.0	−0.1	0.2	−0.1	−0.6
1, 3	−1.2	2.7	0.8	0.0	−1.6	−0.2	0.3	0.0	−0.4	0.1	0.2	0.2	−0.3	0.1	0.8
1, 5	−0.4	0.8	0.6	0.0	−1.1	−0.2	0.3	0.0	0.2	0.0	−0.1	0.1	−0.2	0.0	0.3
1, 9	0.0	0.0	0.0	0.1	0.0	0.0	0.0	0.0	0.0	0.0	0.0	0.0	0.0	0.0	0.1
2, 4	−0.9	−1.6	−1.1	0.0	4.7	0.7	−0.9	−0.2	−0.1	0.0	−0.2	−0.2	0.3	−0.1	−0.4
2, 5	−0.2	−0.2	−0.2	0.0	0.7	0.2	−0.2	0.0	−0.2	0.0	0.0	−0.1	0.1	0.0	−0.1
2, 6	0.2	0.3	0.3	0.0	−0.9	−0.2	0.3	0.0	0.2	0.0	−0.1	0.1	−0.1	0.0	0.1
2, 8	0.1	0.0	0.0	0.0	−0.2	0.0	0.0	0.1	0.0	0.0	0.0	0.1	−0.1	0.0	0.0
3, 4	0.2	−0.4	0.2	0.0	−0.1	−0.2	0.2	0.0	1.2	−0.1	0.0	0.0	0.0	0.0	0.1
3, 7	0.0	0.1	0.0	0.0	0.0	0.0	0.0	0.0	−0.1	0.0	0.0	0.0	0.0	0.0	0.0
4, 6	0.0	0.1	−0.1	0.0	−0.2	0.0	−0.1	0.0	0.0	0.0	0.1	0.0	0.0	0.0	0.0
8, 9	−0.1	0.2	0.1	0.0	−0.2	−0.1	0.1	0.1	0.0	0.0	0.0	0.6	−0.6	−0.1	−0.1
8, 10	0.2	−0.3	−0.2	0.0	0.3	0.1	−0.1	−0.1	0.0	0.0	0.0	−0.6	1.0	−0.4	0.1
9, 10	−0.1	0.1	0.0	0.0	−0.1	0.0	0.0	0.0	0.0	0.0	0.0	−0.1	−0.4	0.5	0.0
Total															0.3

includes a few models for comparison, such as the model with the 10 additive effects and 45 additive-by-additive interaction effects (M_{45}, the starting model in the elimination process), one with the 14 epistatic effects (M_{14}, the selected model), and one with no epistatic term (M_0). Since the likelihood does not decrease as the number of parameters fitted in a model increases, the likelihood for a nested model with more parameters is certainly higher than, or at least as high as, that with fewer parameters. However, when comparing two models, we usually use the likelihood-ratio (LR) test statistic, which is two times the difference between the log likelihoods of the two models (see Table 6), to test for significance. Under nested models, as in this backward elimination process, LR for two models (one with more parameters, usually regarded as the alternative model, and one with fewer parameters, regarded as the null hypothesis) tends to be asymptotically distributed with a χ^2 distribution under the null hypothesis, with the degrees of freedom (d.f.) being the difference in number of parameters. Thus, we may compare the observed LR with $\chi^2_{\text{d.f.},\alpha}$, where α is the significance level to see whether $\text{LR} > \chi^2_{\text{d.f.},\alpha}$ (rejecting the null). (Note that LOD = 0.217 LR.) It is, however, very difficult to decide which α should be used in each comparison because multiple (correlated) tests in multiple steps are involved in this stepwise elimination process. Nevertheless, for Table 6, the decision seems to be relatively easy.

It is clear that the likelihood ratio between M_{45} and M_{14} [the difference between the two log likelihoods denoted as $\text{LR}_{M45:M14}$, which is $2\ln(L_{M45}) - 2\ln(L_{M14}) = 7094 - 7088 = 6 \ll \chi^2_{31,0.1} = 41.2$] is certainly not signifi-

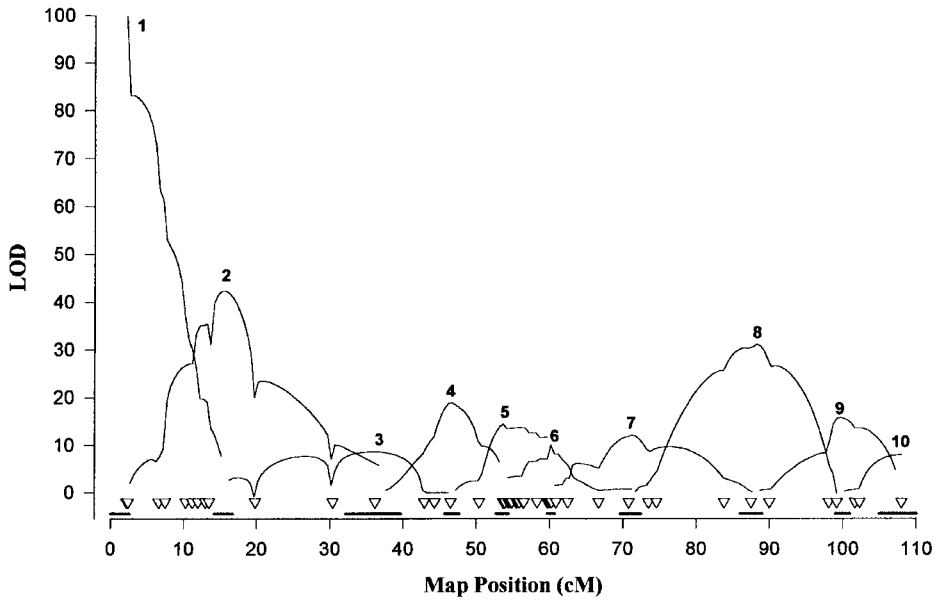

FIGURE 5.—Conditional likelihood profiles of the 10 QTL identified by multiple interval mapping in LOD score. The likelihood profile for each QTL spans from near the estimated position of one neighbor QTL to the other or to the end of the chromosome. The abscissa is in centimorgans (cM) for the linkage map of the markers (indicated by open triangles). Bars indicate the 1-LOD support interval for each QTL, which is the genome region covered by the drop of 1 LOD from the peak in the likelihood profile.

TABLE 6

Statistics of several models in the backward stepwise elimination process for selecting significant QTL epistatic effects

Model	QTL no.	Epistatic effect	2 ln (likelihood)	R^2
M_{45}	10	45	7094	0.952
M_{14}	10	14	7088	0.954
M_{13}	10	13	7075	0.954
M_5	10	5	7058	0.953
M_4	10	4	7041	0.953
M_3	10	3	7008	0.952
M_0	10	0	6997	0.947

cant. Thus, M_{14} is preferred over M_{45} and in fact over any model between M_{14} and M_{45} as even LR = $6 < \chi^2_{1,0.01} = 6.6$. But $LR_{M14:M13}$ ($= 13 > \chi^2_{1,0.0005} = 12.1$) is certainly very significant, and thus M_{14} is preferred over M_{13}. This is why M_{14} was selected in the original analysis. $LR_{M15:M5}$ ($= 12 < \chi^2_{8,0.1} = 13.4$) is not significant. However, $LR_{M14:M5}$ ($= 30 < \chi^2_{9,0.0005} = 29.7$) is very significant. M_5 is significantly different from M_4 ($LR_{M5:M4} = 17 > \chi^2_{1,0.0001} = 15.1$), and M_4 is significantly different from M_3 ($LR_{M4:M3} = 33 > \chi^2_{1,0.0001} = 15.1$). However, M_3 is not significantly different from M_0 ($LR_{M3:M0} = 11 < \chi^{23,0.01} = 11.3$). From this analysis, selecting M_{14} for the final model interpretation seems to be reasonable. If M_{14} were not significantly different from M_{13} (and thus probably also not significantly different from M_5), M_5 would have been selected.

Although only pairwise interaction terms were considered in the search process, higher-order interaction terms, such as the third order involving three QTL, can also be considered in principle. However, to fit a third-order interaction term for three QTL, double recombinants between the three QTL are required for the analysis; otherwise, the analysis will be singular (indicating an overfit of parameters). Although the current data contain double recombinant lines, the number of these lines is still not large enough and the double recombinants are not widespread enough for an effective search for third-order interactions. A search for third-order interactions can easily run into the singularity problem, and even if the analysis is not singular, the test for third-order interaction is unlikely to be significant because of too few double recombinant lines. For these reasons, a search for higher-order interaction terms was not attempted.

Dominance: To assess dominance at loci affecting this trait, males from representative single recombinant lines were crossed to nonrecombinant high- or low-line females in 14 crosses. The single recombinant line nearest the center of the chromosome was crossed to both high and low. The other single recombinant lines were crossed to only high or low. In the resulting hybrids, all loci to one side of the breakpoint are heterozygous and all loci to the other side are homozygous. The phenotypes of parents and their hybrids show the average dominance within blocks of genes (Figure 6). Most heterozygous combinations showed nearly zero dominance, except at one breakpoint on the left arm at ~17 cM in the LH × L crosses.

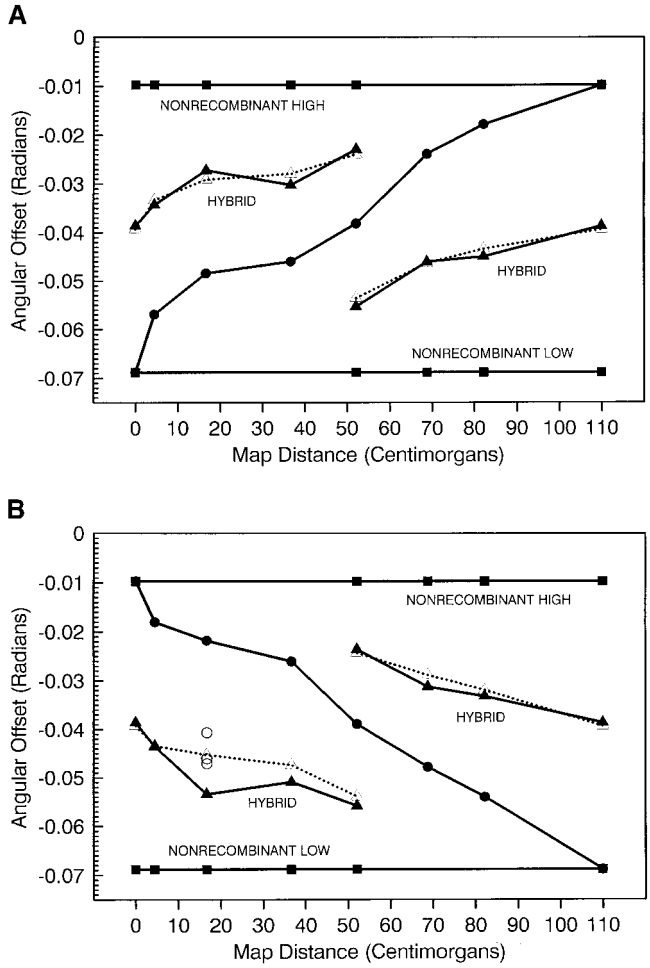

FIGURE 6.—Crosses to assess dominance between high and low alleles. Representative single recombinant lines (●) along the diagonal were crossed to either a high or a low nonrecombinant line (■). The hybrid phenotypes (▲) are always near the midpoint between parental phenotypes (△). All $N = 50$; mean SD = 0.007 rad. (A) Crosses of high-low single recombinants to nonrecombinants. (B) Crosses of low-high single recombinants to nonrecombinants. At 16.7 cM, three additional low-high single recombinant lines were crossed to the same nonrecombinant low line. These hybrids (○) were closer to the midparent value than the first hybrid.

The original LH line used at this breakpoint was lost, so the measurement could not be repeated. Instead, three other LH lines with the same breakpoint and nearly the same mean were crossed to the same low nonrecombinant. Phenotypes of these hybrids are also shown in Figure 6B. The mean of the four hybrid means at this breakpoint reinforces the conclusion that lack of dominance in heterozygotes is typical. There may be a source of atypical variation that affects some recombinants in this interval, however.

TABLE 7

Differences in leg shape between high and low lines

	LHL mean	SD	LLL mean	SD		Base SD	|LHL-LLL|/Base SD
Prothoracic femur	−0.0068	±0.0164	+0.0004	±0.0192	**	0.0153	0.47
Prothoracic tibia	−0.0201	±0.0229	−0.0247	±0.0233	NS	0.0177	0.26
Mesothoracic femur	−0.0145	±0.0214	−0.0165	±0.0199	NS	0.0178	0.11
Mesothoracic tibia	−0.0171	±0.0233	−0.0099	±0.0281	*	0.0206	0.35
Metathoracic femur	+0.0183	±0.0197	+0.0046	±0.0196	***	0.0195	0.70
Metathoracic tibia	−0.0231	±0.0221	−0.0292	±0.0248	*	0.0179	0.34
Wing (index F)	−0.0053		−0.0697			0.0063	10.22

Wings and six leg segments between high and low second chromosome lines are compared (LHL and LLL), using angular offsets from base population allometric baselines, where D_1 = widest segment width and D_2 = narrowest segment width (see MATERIALS AND METHODS). The last column gives absolute values of the differences between LHL and LLL means, divided by the base population phenotypic standard deviation for each trait. Each leg segment mean represents 160 males. NS, not significant. * $P < 0.05$; ** $P < 0.001$; *** $P < 10^{-6}$.

High and low nonrecombinant lines were also crossed reciprocally. This produced indistinguishable hybrid phenotypes with mean and SD of -0.0387 ± 0.008 when sires were high and -0.0384 ± 0.007 when sires were low.

Correlated effects: The previous study (WEBER *et al.* 1999) showed that whole H and L third chromosomes carry genetic differences with small but significant effects on leg segment shape. In the present study, whole H and L second chromosomes were tested for effects on leg segment shapes, as before. As shown in Table 7, the H and L second chromosomes also have significantly different effects on leg segment shape. However, the leg shape differences caused by the second chromosome are even smaller than those reported previously for the third chromosome. [The L-L-L offset for wings is given as −0.0697 here but as −0.0689 in WEBER *et al.* (1999), because each value is the mean of L-L-L nonrecombinant lines arising from a different set of recombination crosses.]

DISCUSSION

Chromosomes 2 and 3 (WEBER *et al.* 1999) appear to be virtually identical in their index F quantitative genetics. Both chromosomes carry many genes affecting this trait. These can be modeled as ~10 factors on each chromosome with small subequal effects dispersed fairly evenly along the recombinational maps. On each chromosome, most of the total effect on genetic variance is due to additive gene action, although many interactions among loci do occur. The net effect of interactions in homozygous recombinants is small and negative across almost every point on both chromosomes. On both chromosomes, heterozygotes are almost exactly intermediate between homozygotes when effects are assayed on a segment-by-segment basis. Finally, each chromosome has detectable effects on leg shape when the whole chromosome is substituted high for low, which might be pleiotropic effects of wing shape genes; but these effects are small.

Chromosome 1 is still being analyzed. With its sex-specific regulation and transmission, it may not fit this picture. We also have no information yet on interactions between chromosomes. Nevertheless, because chromosomes 2 and 3 account for 90% of the phenotypic difference between high and low lines, and in view of the similarity between them, we can attempt to generalize about the quantitative genetics of this wing shape trait.

Number of loci: Multiple interval mapping finds 10 QTL on chromosome 2 and 11 on chromosome 3, while serial *t*-tests find a minimum of nine genes on chromosome 2 and eight on chromosome 3. Thus the original high and low lines differ at ~20 sites affecting this trait. This is a minimum estimate; there is no maximum estimate because of the potential for blocks of closely linked genes. The rather linear relation between cumulative effect and chromosome segment length (Figure 2), and the large numbers of evenly dispersed QTL (Figure 5), could both be manifestations of an underlying continuum of more numerous effects too close together to resolve.

Dominance: Alleles affecting this trait show almost no dominance in heterozygous chromosome segments along both the second chromosome (this study) and the third (WEBER *et al.* 1999). This would also be the expected result if there are large numbers of loci with random amounts of dominance, especially if they tend more often to be semidominant, as is usually the case in quantitative traits (TANKSLEY 1993). Thus our lack of certainty that we have an exhaustive count of loci also affects somewhat our conclusion that alleles are acting with nearly perfect additivity in heterozygotes.

Consistently negative net interactions: In this study and in WEBER *et al.* (1999), the net effect of interactions between loci in homozygous recombinants is negative across almost every point along both major chromosomes. ESHED and ZAMIR (1996) also found widespread negative interactions ("less-than-additive" interactions) in tomatoes among QTL for four fitness traits. They

suggested that these interactions might reflect a partly canalized system that helps to maintain fitness in many diverse genotypes.

Wing shape traits are not strongly canalized against genetic change. They respond to divergent selection in the same way as most quantitative traits—with an immediate response in both directions that is most rapid at the outset (Weber 1990). However, there could still be weak buffering toward wild type that shows up in highly selected genotypes. In our system, where both chromosomes were measured in a low background and all phenotypes were therefore below the presumably optimal range of wild type, the appearance of consistently negative interactions along the whole chromosome would also be generated if gene effects became increasingly less than additive the more they approached wild type. Such a buffering system might result if wing shape were determined by multiple, independent, partially redundant parallel systems, all with selectable variation. At present one can say only that directional asymmetry in the net effects of genetic interactions is strikingly consistent in our studies of wing shape and also in the report of Eshed and Zamir (1996).

Mean effects and net interactions: Figure 7A compares two ways of showing the cumulative effect of genes. The step function (dashed line) shows the cumulative main effects of QTL from Table 3, as computed by MIM using the whole set of recombinant lines. The other curve (solid line) was computed by averaging the two curves of single recombinant lines (HL and LH) from Figure 2. Figure 7B shows net interactions along the chromosome in two ways. Again, the step function shows the net pairwise QTL interactions from MIM (Table 3), while the solid line is the difference between the LH and HL profiles in Figure 2. The fit between the direct empirical averages and the QTL model values in Figure 7 is close and could be improved only by increasing the number of point effects in the QTL model. These comparisons are a useful check on the whole investigation because the two analyses, using different approaches and partly based on different components of the data, were prepared completely independently by K.W. and Z.B.Z. The graphical and statistical analyses do not yield completely equivalent views, but there are close correspondences between them in the distributions of mean effects and net interactions when these are considered separately.

The weakness of net interactions still allows for hidden interactions that are strong. Although the intervals between markers are small, there could conceivably be large interactions between sites so tightly linked that they have no recombinants in this data set. There could also be large interactions that are balanced by other large interactions of equal magnitude and opposite sign if these are distributed in a nonrandom way so that they cancel each other out.

Symmetric pattern of QTL interactions: The locations

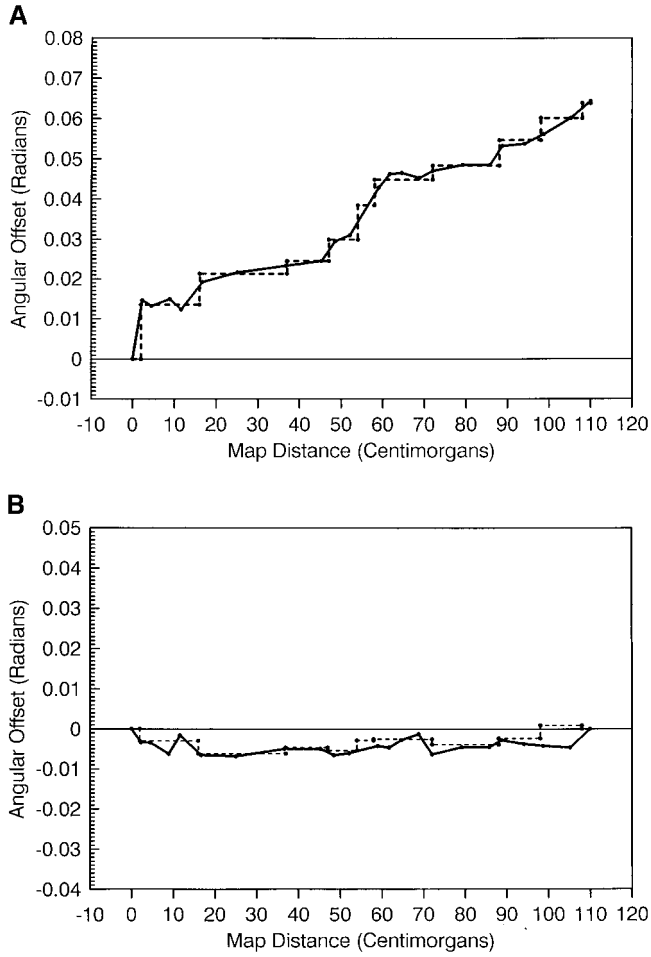

Figure 7.—Comparisons of MIM and graphic analyses of additive and interactive effects along the chromosome. (A) The solid line is the empirical mean cumulative effect along the chromosome based on single recombinants computed by averaging the two curves in Figure 2. The dashed line shows the cumulative total of main effects according to MIM, as listed in Table 3. (B) The solid line shows the difference between the profiles (LH-HL) in Figure 2, representing the magnitude and sign of net interaction across each breakpoint along the chromosome. The dashed line shows the net interaction across each breakpoint according to MIM, computed from the pairwise interactions listed in Table 3.

of the pairwise QTL interactions listed in Table 3 have to be considered along with the magnitudes of their effects. Figure 8 shows how the interactions in Table 3 are arranged along the chromosome. There is a pattern of large, balanced positive and negative effects that nearly cancel each other at every point along the chromosome, leaving only the small residues of net negative effect seen in Figure 7B. The same type of pattern was found in the QTL analysis of chromosome 3. Nevertheless, the phenotypic variation in chromosome 3 could also be explained fairly well ($r^2 = 0.93$) with a model assuming an indefinitely large number of genes acting only independently, *i.e.*, with no interactions (Weber *et al.* 1999).

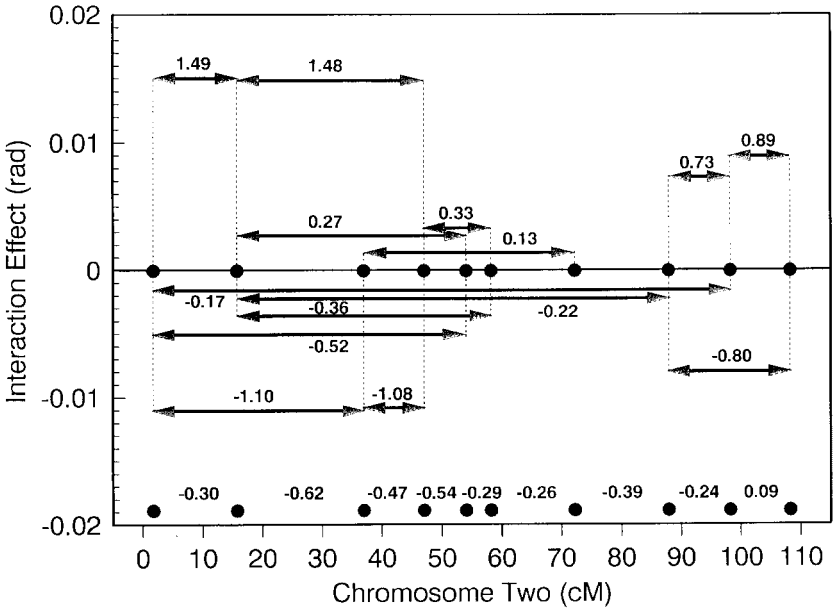

FIGURE 8.—Graphic representation of the pairwise interactions listed in Table 3. The arrows connect pairs of interacting QTL according to MIM, and the elevation of each arrow represents the magnitude of the interaction. The numbers along the bottom show the small residues of net interaction in each interval, equal to the dashed line in Figure 7B.

The apparent balancing of pairwise QTL interactions, found in the MIM analyses of both chromosomes 2 and 3, is highly nonrandom and must be either an effect of natural selection or else perhaps a statistical effect arising in the MIM analysis. If the balanced arrangement is a real effect of natural selection, perhaps it is favored as the pattern that creates the fewest extreme phenotypes, *i.e.*, generates the least phenotypic variance. But this would be a remotely second-order effect. Obviously, we would like more certain confirmation of this phenomenon before venturing too far in search of explanations.

Epistasis in the MIM analysis: Tables 4 and 5 show the partitioning of the genetic variance in the current population of recombinants with a significant amount of linkage disequilibrium among QTL. In this population, the total variance explained by the significant pairwise epistasis is very small compared to the total variance explained by the additive effects (0.3 *vs.* 95.1). This may be somewhat expected because the current recombinant population is created from a cross between high and low selection lines. After intensive divergent selection for 20 generations in large populations, it is likely that most QTL alleles are appropriately fixed in the selection lines; *i.e.*, most plus alleles are in the high line and most minus alleles are in the low line. This is confirmed by the QTL mapping data reported here and in WEBER *et al.* (1999). However, epistatic effects as defined in the model are not necessarily in one direction in this recombinant inbred population. This is because QTL alleles are not necessarily fixed together during the divergent selection. Also, with strong additive effects, some genotype combinations are still favored by selection even with some negative epistatic effects. Furthermore, the genetic structures in the high and low populations during selection are not the same as those in the current recombinant inbred population.

In the population of recombinants in this data set, there is a significant amount of epistatic variation hidden by linkage disequilibrium. As linkage disequilibria among QTL decrease, this component of epistatic variation will be released into the population. For example, in a hypothetical population that has the same genetic structure as the current population except that QTL are in linkage equilibrium, and thus the covariance between different QTL effects reduces to zero, the ratio of the epistatic variation *vs.* the additive variation would be 14.5 *vs.* 45.1 (sums of the diagonals of Table 5 and Table 4 as a percentage of the phenotypic variance in the current population). In this hypothetical population, the majority of the genetic variation would still be due to additive effects of QTL, but the epistatic variation would no longer be negligible.

Pleiotropic effects on shape: In their high and low selected versions, chromosomes 2 and 3 have ~10 times as much effect on wing shape as on leg shape. As shown in Table 7 of this article and in Table 8 of WEBER *et al.* (1999), the wing shape effect in base-population phenotypic standard deviations is 10.22 for chromosome 2 and 9.78 for chromosome 3. By contrast, the mean of all measured shape effects on leg segments (again in base-population standard deviations) is only 0.37 for chromosome 2 and 1.29 for chromosome 3. If one considers only the effects on the mesothoracic leg (of particular interest because it is on the same body segment as the wing) these numbers are even a bit lower, being 0.23 for chromosome 2 and 1.21 for chromosome 3. We conclude from our studies of both chromosomes that, for the traits assayed here, the genetic controls of wing shape and leg shape are largely decoupled from each other. The small, correlated leg shape differences

that are found may be pleiotropic effects of the wing shape genes, or they may simply arise from random fixation at other loci, just as inbreeding in isofemale lines leads to significant differences among lines in wing shape (Weber 1990).

Caveats: These studies tell us much about the genetics of wing shape, but the details are still poorly resolved. We have no upper limit on the number of effects, inadequate constraints on their locations, and great uncertainties about their interactions. We hope our analyses are impeccable as far as they go, but our conclusions are somewhat tentative. If only we could measure an infinite number of lines, the empirical surface of effects would become a step function like the theoretical one, leaving no doubts.

We thank Peter Keightley and two anonymous reviewers for comments. This work was supported by grants from the National Science Foundation (DEB-9407005) to K.W. and from the Public Health Service (GM-45344) to Z-B.Z.

LITERATURE CITED

Birdsall, K., E. Zimmerman, K. Teeter and G. Gibson, 2000 Genetic variation for the positioning of wing veins in *Drosophila melanogaster*. Evol. Dev. **2:** 16–24.

Bookstein, F. L., 1991 *Morphometric Tools for Landmark Data: Geometry and Biology*. Cambridge University Press, New York.

Castle, W. E., 1951 Variation in the hooded pattern of rats, and a new allele of *hooded*. Genetics **36:** 254–266.

Castle, W. E., and J. C. Phillips, 1914 *Piebald Rats and Selection: An Experimental Test of the Effectiveness of Selection and of the Theory of Gametic Purity in Mendelian Crosses*, Pub. No. 195. Carnegie Institute, Washington, DC.

Churchill, G. A., and R. W. Doerge, 1994 Empirical threshold values for quantitative trait mapping. Genetics **138:** 963–971.

Eshed, Y., and D. Zamir, 1996 Less-than-additive epistatic interactions of quantitative trait loci in tomato. Genetics **143:** 1807–1817.

Guerra, D., M. C. Pezzoli, G. Giorgi, F. Garoia and S. Cavicchi, 1997 Developmental constraints in the *Drosophila* wing. Heredity **79:** 564–571.

Kao, C.-H., and Z-B. Zeng, 1997 General formulas for obtaining the MLEs and the asymptotic variance-covariance matrix in mapping quantitative trait loci when using the EM algorithm. Biometrics **53:** 653–665.

Kao, C.-H., Z-B. Zeng and R. Teasdale, 1999 Multiple interval mapping for quantitative trait loci. Genetics **152:** 1203–1216.

Lindsley, D. L., and G. G. Zimm, 1992 *The Genome of Drosophila melanogaster*. Academic Press, San Diego.

Liu, J., J. M. Mercer, L. F. Stam, G. C. Gibson, Z-B. Zeng *et al.*, 1996 Genetic analysis of a morphological shape difference in the male genitalia of *Drosophila simulans* and *D. mauritiana*. Genetics **142:** 1129–1145.

Long, A. D., S. L. Mullaney, L. A. Reid, J. D. Fry, C. H. Langley *et al.*, 1995 High resolution mapping of genetic factors affecting abdominal bristle number in *Drosophila melanogaster*. Genetics **139:** 1273–1291.

Tanksley, S. D., 1993 Mapping polygenes. Annu. Rev. Genet. **27:** 205–233.

Weber, K. E., 1988 A system for rapid morphometry of whole, live flies. Dros. Inf. Serv. **67:** 97–102.

Weber, K. E., 1990 Artificial selection on wing allometry in *Drosophila melanogaster*. Genetics **126:** 975–989.

Weber, K. E., 1992 How small are the smallest selectable domains of form? Genetics **130:** 345–353.

Weber, K. E., R. Eisman, L. Morey, A. Patty, J. Sparks *et al.*, 1999 An analysis of polygenes affecting wing shape on chromosome 3 in *Drosophila melanogaster*. Genetics **153:** 773–786.

Zeng, Z-B., C.-H. Kao and C. J. Basten, 1999 Estimating the genetic architecture of quantitative traits. Genet. Res. **75:** 345–355.

Zimmerman, E., A. Palsson and G. Gibson, 2000 Quantitative trait loci affecting components of wing shape in *Drosophila melanogaster*. Genetics **155:** 671–683.

Communicating editor: P. D. Keightley